

# **Solution processed bilayer photovoltaic devices with nematic liquid crystals**

Manea S AlKhalifah<sup>†</sup> Chunhong Lei, Steven A Myers and Mary O'Neill,\*

*Department of Physics and Mathematics, University of Hull, Hull, HU6 7RX, U.K.*

Stuart P Kitney and Stephen M Kelly,\*

*Department of Chemistry, University of Hull, Hull, HU6 7RX, U.K.*

[m.oneill@hull.ac.uk](mailto:m.oneill@hull.ac.uk); [s.m.kelly@hull.ac.uk](mailto:s.m.kelly@hull.ac.uk)

<sup>†</sup>Current address: Department of Physics, College of Science and Art at Alrass, Qassim University, Kingdom of Saudi Arabia.

# **Solution processed bilayer photovoltaic devices with nematic liquid crystals**

The crosslinking of polymerisable liquid crystalline semiconductors is a promising approach to solution processable, multilayer, organic photovoltaics. Here we demonstrate an organic bilayer photovoltaic with an insoluble electron donating layer formed by crosslinking a nematic reactive mesogen. We investigate a range of perylene diimide materials, some of which are liquid crystalline, as the overlying electron acceptor layer. We find that the carrier mobility of the acceptor materials is enhanced by liquid crystallinity and that mobility limits performance of the photovoltaic devices.

Liquid crystals, photovoltaics, bilayer, crosslinking, reactive mesogen, perylene, bulk heterojunction. .

## **1. Introduction**

There is increasing interest in the development of organic photovoltaics based on charge separation at the interface between electron donating and accepting organic materials.

There are two distinct processing routes to organic photovoltaics; solution processing of polymeric materials[1, 2] and thermal evaporation of small molecules.[3] The latter allows the fabrication of more sophisticated multiple layers devices whilst the former, although more suitable for low cost manufacturing, requires deposition from incompatible solvents to build multilayer devices. The bulk heterojunction device, in which photogenerated electrons and holes are disassociated within a thin film of a phase-separated blend of donor and acceptor materials, was invented to optimise efficiency in a single active layer.[1, 2, 4-8] However multi-layer configurations have added functionality such as carrier and exciton blocking layers to prevent quenching of

the two species at the electrodes.[9, 10] The tandem device, in which two or more devices are superimposed to increase the spectral coverage or absorption length, is a very promising approach to further increase the efficiency of organic photovoltaics.[11]

The polymerization and crosslinking of reactive mesogens is a promising approach to multi-layer devices based on solution processing. Reactive mesogens are similar to small molecule LCs, but with two additional polymerizable groups, one at each end of a flexible aliphatic spacer attached to the aromatic core. Thin films can be formed by solution processing, Nematic reactive mesogens adopt a planar alignment with the long molecular axis aligned in the substrate plane.[12] They can be uniaxially aligned using rubbing or photoalignment techniques resulting in very high order parameters particularly for materials with extended molecular cores.[13-15] Polymerization and crosslinking occur either by the thermal or photoinduced generation of free radicals using ultraviolet light or by ionic photoinitiation resulting in insoluble thin films.[14, 16-18] Photopolymerisation offers the further advantage of pixellation by photolithography: unexposed regions are simply removed by washing in the original spin-casting solvent. Previously we have investigated the light-emission and charge transporting properties of a class of semiconducting nematic reactive mesogens.[19, 20] which are to create a **D-A** bilayer with a distributed interface.[21-23]

In this paper we report on bilayer and bulk heterojunction photovoltaics using liquid crystalline reactive mesogen donors and a range of acceptors with perylene diimide groups combined with fluorene or carbazole moieties. The acceptors are characterized optically and electronically. We show that the acceptor molecules studied have no measurable charge transfer characteristics. The electron and hole mobility is enhanced when the acceptors have liquid crystalline phases. The efficiency of a photovoltaic

blend is not affected by ultraviolet photopolymerisation of the active bulk heterostructure layer. Bilayer devices are investigated to identify the parameters which limit performance.

## 2. Experimental Section

### 2.1 Materials Synthesis.

The perylene **1** was prepared as reported previously.[22] The perylene **2** exhibits a symmetrical A-B-A molecular structure with a fluorene moiety decoupled by a short aliphatic spacer from the perylene core. It was prepared by a short convergent synthesis shown in reaction scheme 1. The perylene **3** was synthesized as shown in reaction scheme 2. The perylene **4** was synthesized as shown in reaction scheme 3. The perylene **5** is very similar in shape to compound **1** and was prepared in a similar fashion according to a modified literature method as shown in reaction scheme 4.[22] Compound **5** has a carbazole moiety in place of the fluorene moiety in compound **1** and has a branched aliphatic (nonadecyl) chain in place of the two octyl chains in compound **5**. The perylene **6** was synthesized in a similar fashion to perylene **4** as shown in reaction scheme 5. The liquid crystalline and electron-donating monomer **7** (a reactive mesogen) with two terminal substituents comprising a methacrylate photopolymerisable group at the end of an aliphatic spacer joined to the aromatic core was synthesised according to a modified literature method.[22]

[Insert schemes 1-5 here]

The structures of intermediates and final products were confirmed by proton (<sup>1</sup>H) nuclear magnetic resonance (NMR) spectroscopy (JOEL JMN-GX270 FT nuclear resonance spectrometer), infra-red (IR) spectroscopy (Perkin Elmer 783 infra-red

spectrophotometer) and mass spectrometry (MS) (Finnegan MAT 1020 automated GC/MS). Reaction progress and product purity was checked using a CHROMPACK CP 9001 capillary gas chromatograph fitted with a 10 m CP-SIL 5CB (0.12  $\mu\text{m}$ , 0.25 mm) capillary column. All of the final products were more than 99.5% pure by GLC. Transition temperatures were determined using an Olympus BH-2 polarising light microscope together with a Mettler FP52 heating stage and a Mettler FP5 temperature control unit. The analysis of transition temperatures and enthalpies was carried out by a Perkin-Elmer DSC7-PC differential scanning calorimeter. The octyloxy chain was used as a protecting group during the synthesis of compound **1** as the starting material for scheme 1 because it was available from another programme and longer chains are easier to remove than shorter ones. We now usually use branched alkoxy chains, such as citronenyloxy groups, since they act as a better protecting group in terms of lowering the melting point of the reaction intermediates and increasing their solubility in organic solvents.

## ***2.2 Analytical Methods.***

The ionization potential (IP) and electron affinity (EA) of the materials were measured electrochemically in solution by cyclic voltammetry (CV) using a computer-controlled scanning potentiostat (Solartron 1285). 1 mM of the compound was dissolved in an electrolytic solution of 0.3M tetrabutylammonium hexafluorophosphate in dichloromethane. The solution was placed in a standard three-electrode electrochemical cell. A glassy carbon electrode was used as the working electrode. Saturated silver/silver chloride and platinum wire formed the reference and counter electrodes respectively. The electrolyte was recrystallized twice before use and oxygen contamination was avoided by purging the solution with dry nitrogen before each

measurement. The measured potentials were corrected using an internal ferrocene reference added at the end of each measurement. The onset potential for oxidation (reduction),  $E_{ox}^{onset}$  ( $E_{red}^{onset}$ ), were estimated from the intersection of the two tangents at the rising (descending) oxidation (reduction) current and the background current respectively in the cyclic voltammogram. We use the relationships

$$IP(eV) = E_{ox}^{onset} + 4.7 + \delta; EA(eV) = E_{red}^{onset} + 4.7 + \delta \quad (1)$$

since the potential of the Ag/AgCl electrode is 4.7 eV with respect to the vacuum.[24, 25]  $\delta$  is a calibration parameter equal to  $0.425 - E_{Fc-M}^{1/2}$ , where  $E_{Fc-M}^{1/2}$  is the measured half-wave potential of the ferrocene oxidation peak.[26]

The charge carrier mobility was measured using the photocurrent time-of-flight method. Thick samples (1-2  $\mu\text{m}$ ) of each of the materials were prepared by spin-casting from a solution of concentration 50 -100 mg/ml of toluene onto an Indium Tin Oxide substrate. The substrate was uniformly coated with the filtered (0.2  $\mu\text{m}$ ) solution. After lying for  $\approx$  20 minutes in a solvent rich environment, the samples were spun at 900 rpm for 30s, with an acceleration of 590 rpm<sup>2</sup>. They were dried in a vacuum and an Al electrode deposited on top. A Wyko white-light interferometer (Wyko NT1100) was used to measure the film thickness  $d$ . A Laser Science Inc. VSL-337ND Nitrogen laser with pulses of wavelength 337 nm and 6 ns duration optically pumped the sample, which was maintained in an inert environment. A uniform electric field was applied across the organic layer and the photocurrent was measured as a function of time using LABVIEW controlled software. The transit time,  $\tau$ , was obtained from the intercept of the photocurrent plateau and tail, plotted on a logarithmic scale. The carrier mobility,  $\mu$ , is obtained from the equation  $\mu=d/(E\tau)$ . Molecular mechanics using MM2 energy minimisation was carried out to obtain the orbital wavefunctions of compounds. ChemBio3D Ultra software was used.

### 2.3. Device Fabrication.

Indium-tin oxide (ITO, 13 $\Omega$ ) coated glass was used as substrates for the photovoltaic devices. The substrates were first etched in an oxygen plasma (0.5 mbar, 1W, 10min). Polystyrene sulphonate/polyethylene dioxythiophene (PSS/PEDOT, Baytron P VP Al 4083) was deposited by spin-casting at 4000rpm. The PSS/PEDOT layer was baked at 160 °C for 30 minutes. For the bilayer devices, the cross-linkable donor material was spin-coated from a chlorobenzene solution onto the PSS/PEDOT surface and cross-linked by irradiation using light from a HeCd laser at 325 nm, using a total fluence of 300 J cm<sup>-2</sup>. After washing the film with chlorobenzene, the acceptor layer was spin-coated on top. The blend device contained a blended layer consisting of an equal fraction of **7** and **1** by weight spin-cast from a 1.5 weight % solution in chlorobenzene. The films were then annealed at 120 °C for 60 mins. All these were done in a nitrogen glover-box. As a top electrode, 0.6 nm of lithium fluoride (LiF) followed by 60 nm of aluminum was deposited through a mask. The devices were illuminated with a Xenon lamp, dispersed through a monochromator and attenuated with neutral light filters over an area of 0.25cm<sup>2</sup>. The current-voltage characteristics of the photovoltaic devices were measured in an inert atmosphere using a Visual-Basic controlled picoammeter.

### 2.4. Experimental Details.

**2-(4-Bromobutyl)-9,9-dioctylfluorene (9)** A solution of *n*-butyllithium (10.65 cm<sup>3</sup>, 2.5 M, 26.60 mmol) was added dropwise to a cooled (0 °C) solution 2-bromo-9,9-dioctylfluorene (10.00 g, 21.33 mmol) in diethyl ether (200 cm<sup>3</sup>). The mixture was stirred for 1 hr while maintaining the temperature then the reaction mixture rapidly quenched with 1,4-dibromobutane (22.99 g, 106.50 mmol). The solution was allowed to

gradually warm to room temperature then heated under reflux for 4 h. The cooled reaction mixture was quenched with water (100 cm<sup>3</sup>) and the product extracted into hexane (3 x 100 cm<sup>3</sup>). The combined organic extracts were washed with brine (3 x 50 cm<sup>3</sup>) dried (MgSO<sub>4</sub>), filtered and concentrated under reduced pressure. The excess 1,4-dibromobutane was removed using Kugelrohr distillation and the remaining oil purified using column chromatography to yield a colourless oil (6.9 g, 62%). <sup>1</sup>H NMR (400 MHz, CDCl<sub>3</sub> δ): 7.52 – 7.56 (4H, m), 7.44 – 7.49 (3H, m) 3.44 (3H, t, j = 7.0 Hz), 2.64 (2H, t, j = 7.0 Hz), 1.86 – 1.92 (2H, m), 1.72 – 1.80 (2H, m). MS (EI) (*m/z*): 525 (M<sup>+</sup>).

**2-[4-(9,9-Dioctylfluoren-2-yl)butyl]isoindoline-1,3-dione (11)** A mixture of potassium phthalamide (**10**) (2.20 g, 11.89 mmol), 2-(4-bromobutyl)-9,9-dioctylfluorene (**9**) (5.00 g, 9.50 mmol) and toluene (100 cm<sup>3</sup>) was stirred under reflux overnight. The cooled reaction mixture was poured into water (100 cm<sup>3</sup>) and the crude product extracted into diethyl ether (3 x 50 cm<sup>3</sup>). The combined organic extracts were washed with brine (2 x 50 cm<sup>3</sup>) dried (MgSO<sub>4</sub>), filtered and concentrated under reduced pressure. The crude product was purified using column chromatography (silica gel, dichloromethane, Hexane, 1:1) and recrystallisation from ethanol to yield a white crystalline solid (2.9 g, 51%). <sup>1</sup>H NMR (400 MHz, CDCl<sub>3</sub> δ): 7.53 – 7.56 (4H, m), 7.44 – 7.51 (3H, m) 3.75 (2H, t, j = 6.5 Hz), 2.65 (2H, t, j = 6.0 Hz), 1.98 (2H, pent), 1.77 – 1.88 (2H, m). MS (EI) (*m/z*): 591 (M<sup>+</sup>).

**4-(9,9-Dioctylfluoren-2-yl)butan-1-amine (12)** A mixture of 2-[4-(9,9-dioctylfluoren-2-yl)butyl]isoindoline-1,3-dione (**11**) (2.00 g, 3.38 mmol) hydrazine hydrate (25 cm<sup>3</sup>)



and ethanol (100 cm<sup>3</sup>) was heated under reflux for 3 h, then allowed to cool to RT. The reaction mixture was concentrated under reduced pressure and the crude product triturated with hexane to yield a yellow waxy solid (quantative yield, 1.6 g). The product was used without further purification due the unstable nature of alkyl amines.

<sup>1</sup>H NMR (400 MHz, CDCl<sub>3</sub> δ): 7.50 – 7.55 (4H, m), 7.44 – 7.49 (3H, m), 2.71 (2H, t, j = 7.5 Hz), 2.62 (2H, t, j = 7.5 Hz), 1.65 (2H, pent), 1.47 (2H, pent), 1.29 (2H, br, s). MS (EI) (*m/z*): 461 (M<sup>+</sup>).

**Compound 2.** A mixture of 3,4,9,10-perylene tetracarboxylic dianhydride (**13**) (0.21 g, 0.542 mmol) 4-(9,9-dioctylfluoren-2-yl)butan-1-amine (**12**) (1.00 g, 2.166 mmol) zinc acetate dihydrate (0.06 g, 0.268 mmol) and dimethylacetamide (50 cm<sup>3</sup>) was heated (160 °C) overnight. The cooled reaction mixture was poured into methanol (50 cm<sup>3</sup>) and the resulting precipitate filtered then purified by column chromatography on silica gel and recrystallised from dichloromethane/dimethylsulfoxide to yield a red crystalline solid (0.37 g, 54%). <sup>1</sup>H NMR (400 MHz, CDCl<sub>3</sub> δ): 8.77 (4H, d, j = 7.9 Hz), 8.66 (4H, d, j = 8.1 Hz), 7.52 – 7.56 (10H, m), 7.44 – 7.49 (6H, m), 4.21 (4H, t, j = 7.7 Hz), 1.86 (4H, pent), 1.71 (4H, pent). MS HABA (*m/z*): 1279.256. Anal. Calcd C: 84.86, H: 8.35, N: 2.19. Anal. Obt. C: 84.94, H: 8.33, N: 2.05.

**2-Bromo-7-iodo-9,9-dioctylfluorene (15).** Powdered potassium hydroxide (4.69 g, 83.6 mmol) was added in small portions to a solution of 2-bromo-7-iodofluorene (**14**) (7.30 g, 19.7 mmol), 1-bromooctane (7.98 g, 41.3 mmol), potassium iodide (0.33 g, 1.97 mmol) and dimethyl sulfoxide (140 cm<sup>3</sup>) at room temperature. The resultant

mixture was stirred for 3 h then poured into water (300 cm<sup>3</sup>). The crude product was extracted into hexane (4 x 100 cm<sup>3</sup>) and the combined organic extracts washed with dilute hydrochloric acid (20%, 100 cm<sup>3</sup>) and brine (2 x 100 cm<sup>3</sup>). The organic layer was dried (MgSO<sub>4</sub>), filtered and concentrated under reduced pressure. Purification of the crude product was carried out by recrystallisation from ethanol to yield a white crystalline solid (11.72 g, 92%). <sup>1</sup>H NMR (400 MHz, CDCl<sub>3</sub> δ): 7.64 – 7.66 (2H, m), 7.52 (1H, dd, j = 7.9, 0.8 Hz), 7.39 – 7.46 (3H, m), 1.87 – 1.92 (4H, m), 1.05 – 1.26 (20H, m), 0.83 (6H, t, j = 7.0 Hz), 0.55 – 0.61 (4H, m) MS (EI) (*m/z*): 594 (M<sup>+</sup>).

**2-Bromo-7-(4-methoxyphenyl)-9,9-dioctylfluorene (17).** A mixture of 2-bromo-7-iodofluorene-9,9-dioctylfluorene (**15**) (10.00 g, 16.78 mmol), 4-methoxyphenyl boronic acid (**16**) (2.93 g, 19.30 mmol), potassium carbonate (5.80 g, 41.99 mmol), palladium tetrakis(triphenyl phosphine) (0.97 g, 0.840 mmol) and tetrahydrofuran (68 cm<sup>3</sup>) was heated at 80 °C overnight. The cooled reaction mixture was poured into methanol (50 cm<sup>3</sup>) and the resulting precipitate filtered and purified using column chromatography on silica gel using 3:2 mixture of hexane and dichloromethane as eluent and recrystallised from ethanol to yield a yellow precipitate (6.33 g, 66%) <sup>1</sup>H NMR (CDCl<sub>3</sub> δ): 7.76 (1H, d, j = 0.92 Hz), 7.74 (1H, d, = 8.8 Hz), 7.61 – 7.66 (4H, m), 7.48 (1H, dd, j = 8.0, 1.1 Hz), 7.35 (1H, d, j = 8.0 Hz), 6.98 (2H, d, j = 8.8 Hz), 3.43 (3H,s), 2.01 – 2.09 (4H, m), 1.04 – 1.28 (24H, m), 0.82 (6H, t, j = 5.4 Hz). MS (*m/z*): 576 (M<sup>+</sup>).

**4-[7-(4-Methoxyphenyl)-9,9-dioctylfluoren-2-yl]-phenylamine (19).** A mixture of 2-bromo-7-(4-methoxyphenyl)-9,9-dioctylfluorene (**17**) (3.25 g, 5.65 mmol) 4-(4,4,5,5-

tetramethyl-1,3,2 dioxborolan-2-yl aniline (**18**) (1.24 g, 5.65 mmol), palladium tetrakis(triphenyl phosphine) (0.33, 0.282 mmol), potassium phosphate (1.80 g, 8.47 mmol) and degassed dimethylformamide (40 cm<sup>3</sup>) was heated at 80 °C overnight. The cooled reaction mixture was poured into water (50 cm<sup>3</sup>) and the crude product extracted into diethyl ether (3 x 100 cm<sup>3</sup>). The combined extracts were washed with dilute hydrochloric acid (20%, 100 cm<sup>3</sup>) and brine (2 x 100 cm<sup>3</sup>), dried (MgSO<sub>4</sub>), filtered and concentrated under reduced pressure. The crude product was purified by column chromatography on silica gel using a 1:1 mixture of hexane and dichloromethane as eluent to yield a yellow waxy solid (2.65 g, 80%). <sup>1</sup>H NMR (400 MHz CDCl<sub>3</sub> δ): 7.72 (1H, d, j = 3.3 Hz), 7.70 (1H, d, j = 3.3 Hz), 7.61 (2H, d, j = 8.8 Hz), 7.49 – 7.52 (6H, m), 7.01 (2H, d, j = 8.8 Hz), 6.79 (2H, d, j = 8.6 Hz), 3.88 (3H, s), 1.98 – 2.02 (4H, m), 1.05 – 1.19 (20H, m), 0.79 (6H, t, j = 7.0 Hz), 0.68 – 0.73 (4H, m). MS (EI) (*m/z*): 588 (M<sup>+</sup>).

**Compound 3.** A mixture of 3,4,9,10-perylene tetracarboxylic dianhydride (**13**) (0.45 g, 1.10 mmol) 4-[7-(4-methoxyphenyl)-9,9-dioctylfluoren-2-yl] phenylamine (**19**) (1.14 g, 2.30 mmol) zinc acetate dihydrate (0.13 g, 0.574 mmol) and imidazole (8.00 g) was heated at 160 °C overnight. The cooled reaction mixture was extracted into dichloromethane (4 x 50 cm<sup>3</sup>) and the resulting solution filtered to remove precipitate formed. The filtrate was concentrated under reduced pressure and the crude product purified by column chromatography on silica gel using dichloromethane as eluent and recrystallised from a mixture dichloromethane and dimethyl sulphoxide to yield a red crystalline solid (1.31 g, 74%). <sup>1</sup>H NMR (400 MHz CDCl<sub>3</sub> δ): 8.65 (4H, d, j = 7.7 Hz), 8.55 (4H, d, j = 8.1 Hz), 7.79 (4H, d, j = 8.2 Hz), 7.67 (4H, dd, j = 7.6, 5.1 Hz), 7.54 –

7.57 (8H, m), 7.48 (4H, d,  $j = 8.8$  Hz), 7.41 (4H, d,  $j = 8.8$  Hz), 6.95 (4H, d,  $j = 8.6$  Hz), 3.81 (6H, s), 1.97 – 1.98 (8H, m), 1.01 – 1.13 (40H, m), 0.73 (12H, t,  $j = 7.0$  Hz), 0.66 – 0.68 (8H, m). MS (HABA) ( $m/z$ ): 1531.231 Anal. Calc. C: 84.67, H: 7.24, N: 1.83, Anal. Obt. C:84.37, H: 7.30, N: 1.75. Cr - N = 285 °C; N - I = >350 °C.

**2-Bromo-7-nitro-9,9-dioctylfluorene (21).** Powdered potassium hydroxide (15.62 g, 278.30 mmol) was added in small portions over 30 min to a mixture of 2-bromo-7-nitrofluorene (**20**) (19.00 g, 65.50 mmol), 1-bromooctane (27.83 g, 144.10 mmol) potassium iodide (1.09 g, 6.55 mmol) and dimethyl sulphoxide (280 cm<sup>3</sup>) at RT. The solution was stirred for 4 h then poured into water (400 cm<sup>3</sup>). The crude product was extracted into ethyl acetate (4 x 100 cm<sup>3</sup>). The combined organic extracts were washed with dilute hydrochloric acid (20%, 100 cm<sup>3</sup>) and brine (2 x 200 cm<sup>3</sup>), then dried (MgSO<sub>4</sub>), filtered and concentrated under reduced pressure. Purification of the crude product was carried out by recrystallisation from ethanol to yield yellow needles (22.37 g, 66%). <sup>1</sup>H NMR (400 MHz, CDCl<sub>3</sub>  $\delta$ ): 8.25 (1H, d,  $j = 2.2$  Hz), 8.23 (1H, d,  $j = 2.0$  Hz), 7.80 (1H, dd,  $j = 7.5, 1.1$  Hz), 7.77 – 7.83 (3H, m) MS (EI) ( $m/z$ ): 513 (M<sup>+</sup>).

**4,4,5,5-Tetramethyl-2-(7-nitro-9,9-dioctylfluoren-2-yl)-[1,3,2]-dioxaborolane (24).**

Pd(dppf)Cl<sub>2</sub> (0.29 g, 0.389 mmol) was added to a degassed solution of 2-bromo-9,9-dioctylfluorene (**21**) (10.00 g, 19.40 mmol), bis(pinacolato)diboron (5.43 g, 21.38 mmol), potassium acetate (5.72 g, 58.28 mmol) and dimethyl sulphoxide (97 cm<sup>3</sup>). The mixture was heated overnight at 80 °C, allowed to cool to RT then poured into water

(300 cm<sup>3</sup>). The crude product was extracted into ethyl acetate (3 x 100 cm<sup>3</sup>) and the combined organic extracts were washed with brine (2 x 100 cm<sup>3</sup>), dried (MgSO<sub>4</sub>), filtered and concentrated under reduced pressure. Purification of the crude product was carried out by column chromatography on silica gel using a 3:2 mixture of hexane and dichloromethane as eluent to yield a yellow waxy solid (7.65 g, 70%). <sup>1</sup>H NMR (400 MHz, CDCl<sub>3</sub> δ): 8.27 (1H, d, j = 2.2 Hz), 8.25 (1H, d, j = 2.0 Hz), 7.86 (1H, dd, j = 7.6, 0.9 Hz), 7.77 – 7.83 (3H, m), 2.02 – 2.07 (4H, m), 1.40 (12H, s), 1.02 – 1.78 (22H, m), 0.81 (6H, t, j = 6.9 Hz), 0.49 – 0.60 (4H, m). MS (EI) (*m/z*): 561 (M<sup>+</sup>).

**7-Nitro-9,9-dioctyl-9',9'-dipentyl-[2,2']-bifluorene (25).** A mixture of 4,4,5,5-tetramethyl-2-(7-nitro-9,9-dioctylfluoren-2-yl)-[1,3,2]-dioxaborolane (**24**) (3.50 g, 6.23 mmol), 2-bromo-9,9-dipentylfluorene (**23**) (2.40 g, 6.23 mmol), tetrakis palladium triphenylphosphine (0.22 g, 0.19 mmol) potassium phosphate (1.98 g, 9.33 mmol) and dimethyl formamide (45 cm<sup>3</sup>) was heated at 80 °C overnight. The reaction mixture was allowed to cool to room temperature and poured into methanol (50 cm<sup>3</sup>). The resulting precipitate was filtered and purified by column chromatography on silica gel using a 3:2 mixture of dichloromethane and hexane as eluent to yield an orange crystalline solid (2.01 g, 43%). <sup>1</sup>H NMR (400 MHz, CDCl<sub>3</sub> δ): 8.21 – 8.27 (2H, m), 7.60 – 7.85 (8H, m), 7.33 – 7.40 (3H, m), 2.01 – 2.06 (8H, m), 1.07 – 1.26 (36H, m), 0.69 – 0.80 (12H, m). MS (EI) (*m/z*): 739 (M<sup>+</sup>).

**9,9-Dioctyl-9',9'-dipentyl-[2,2']-bifluorenyl-7-ylaniline (26).** Tin chloride dihydrate (3.43 g, 15.20 mmol) was added to solution of 7-nitro-9,9-dioctyl-9',9'-dipentyl-[2,2']-

bifluorene (**25**) (2.25 g, 3.00 mmol) and ethanol (250 cm<sup>3</sup>) and the mixture heated under reflux for 6 h. The cooled reaction mixture was filtered through a celite pad and the celite washed with dichloromethane (5 x 50 cm<sup>3</sup>). The filtrate was concentrated under reduced pressure and the crude product used without further purification due to the unstable nature of aromatic amines and the high conversion yield (2.05 g, 95%). <sup>1</sup>H NMR (400 MHz, CDCl<sub>3</sub> δ): 7.72 – 7.77 (2H, m), 7.50 – 7.63 (6H, m), 7.30 – 7.35 (3H, m), 6.66 – 6.69 (2H, m), 2.00 – 2.03 (8H, m), 1.07 – 1.21 (36H, m), 0.70 – 0.83 (12H, m). MS (HABA) (*m/z*): 709.661 (M<sup>+</sup>).

**Compound (4).** A mixture of 3,4,9,10-perylene-tetracarboxylic dianhydride (**13**) (0.50 g, 1.30 mmol) 9,9-dioctyl-9',9'-dipentyl-[2,2']-bifluorenyl-7-ylaniline (**26**) (1.90 g, 2.70 mmol) zinc acetate dihydrate (0.14 g, 0.637 mmol) and imidazole (10.00 g) was heated at 160 °C overnight. The cooled reaction mixture was dissolved in dichloromethane (4 x 50 cm<sup>3</sup>) and the resultant solution filtered to remove the precipitate formed. The filtrate was concentrated under reduced pressure and the crude product purified by column chromatography on silica gel using dichloromethane as the eluent and recrystallisation from a mixture of dichloromethane and dimethyl sulphoxide to yield a red crystalline solid (1.17 g, 52%). <sup>1</sup>H NMR (400 MHz, CDCl<sub>3</sub> δ): 8.81 (4H, d, *j* = 7.9 Hz), 8.73 (4H, d, *j* = 8.1 Hz), 7.92 (2H, d, *j* = 8.4 Hz), 7.85 (2H, d, *j* = 7.9 Hz), 7.79 (2H, d, *j* = 7.7 Hz), 7.75 (2H, d, *j* = 6.4 Hz), 7.64 – 7.70 (8H, m), 7.32 – 7.38 (8H, m), 2.01 – 2.06 (16H, m), 1.07 – 1.22 (40H, m), 0.72 – 0.90 (40H, m). MS (HABA) (*m/z*): 1776.201 Anal. Calc. C: 86.54, H: 8.28, N: 1.58, Anal. Obt. C: 86.47, H: 8.50, N: 1.51. MP. 261 °C

**9-(1-Octylnonyl)-carbazol-2-ylamine (30).** Tin chloride dihydrate (2.25 g, 10.00 mmol) was added to solution of 9-(heptadecan-9-yl)-2-nitro-carbazole (**29**) (0.90 g, 2.00 mmol) and ethanol (50 cm<sup>3</sup>) and the mixture heated under reflux for 6 h. The cooled reaction mixture was filtered through a celite pad and the celite washed with dichloromethane (5 x 50 cm<sup>3</sup>). The filtrate was concentrated under reduced pressure and the crude product used without further purification due to the unstable nature of aromatic amines and the high conversion yield, which gave a yellow crystalline solid (0.83 g, 99%). HABA (*m/z*): 420.114 Anal. Calc. C: 82.80, H: 10.54, N: 6.66, Anal. Obt. 82.62, H: 10.37, N: 6.44.

**Compound (5).** A mixture of 3,4,9,10-perylene-tetracarboxylic acid dianhydride (**13**) (0.19 g, 0.484 mmol) 9-(1-octylnonyl)-carbazol-2-ylamine (**30**) (0.81 g, 1.90 mmol) zinc acetate dihydrate (0.05 g, 0.242 mmol) and imidazole (10.00 g) was heated at 160 °C overnight. The cooled reaction mixture was extracted into dichloromethane (4 x 50 cm<sup>3</sup>) and the resulting solution filtered to remove precipitate formed. The filtrate was concentrated under reduced pressure and the crude product purified by column chromatography [silica gel, dichloromethane] and recrystallised from a mixture of dichloromethane and dimethyl sulphoxide to yield a red crystalline solid (0.35 g, 60%). <sup>1</sup>H NMR (400 MHz, CDCl<sub>3</sub> δ): 8.75 (4H, s, br), 8.56 (4H, s, br), 8.26 (2H, m, br), 8.14 (2H, m, br), 7.58 – 7.68 (2H, m, br), 7.40 – 7.50 (4H, br, m), 7.16 – 7.28 (4H, m, br), 4.50 – 4.60 (2H, m, br), 2.20 – 2.30 (4H, m, br), 1.80 – 2.00 (4H, m, br), 1.10 – 1.30 (40H, m), 0.83 (12H, t, *j* = 7.3 Hz). MS(HABA) (*m/z*): 1196.87 Anal. Calc. C: 82.24, H: 7.74, N: 4.68, Anal. Obt. C: 82.11, H: 8.03, N: 4.38. MP. 348 °C.

**7-(Methoxyphenyl)-7'-nitro-9,9,9',9'-tetraoctyl-[2,2']-bifluorene (31).** Tetrakis palladium triphenylphosphine (0.20 g, 0.174 mmol), was added to a degassed mixture of 2-bromo-7-(4-methoxyphenyl)-9,9-dioctylfluorene (**17**) (2.00 g, 3.50 mmol), 4,4,5,5-tetramethyl-2-(7-nitro-9,9-dioctylfluoren-2-yl)-[1,3,2]-dioxaborolane (**24**) (2.15 g, 3.80 mmol), potassium phosphate (1.60 g, 5.20 mmol) and dimethyl formamide (15 cm<sup>3</sup>). The mixture was heated at 80 °C overnight, allowed to cool and the mixture concentrated under reduced pressure. The crude product was purified by column chromatography on silica gel using a 3:2 mixture of hexane and dichloromethane to yield a yellow waxy solid (2.46 g, 76 %). <sup>1</sup>H NMR (400 MHz, CDCl<sub>3</sub> δ): 8.30 (1H, dd, j = 8.3, 2.2 Hz), 8.23 (1H, d, j = 2.2 Hz), 7.77 – 7.87 (4H, m), 7.65 – 7.76 (6H, m), 7.54 – 7.58 (2H, m), 7.02 (2H, d, j = 8.8 Hz). 3.86 (3H,s), 1.94 – 2.06 (8H, m), 1.08 – 1.26 (40H, m), 0.77 – 0.83 (20H, m). MS (HABA) (*m/z*): 930.39.

**7'-(4-Methoxyphenyl)-9,9,9',9'-tetraoctyl-[2,2']-bifluorenyl-7-ylamine (32).** Tin chloride dihydrate (2.98 g, 13.20 mmol) was added to solution of 7-(methoxyphenyl)-7'-nitro-9,9,9',9'-tetraoctyl-[2,2']-bifluorene (**31**) (2.46 g, 2.60 mmol) and ethanol (200 cm<sup>3</sup>) and the mixture heated under reflux for 6 h. The cooled reaction mixture was filtered through a celite pad, which was then washed with dichloromethane (7 x 50 cm<sup>3</sup>). The combined filtrate was concentrated under reduced pressure. The crude product obtained was used without further purification due to the unstable nature of aromatic amines and the high conversion yield, which gave a yellow crystalline solid in near quantitative yield (2.18 g). <sup>1</sup>H NMR (400 MHz, CDCl<sub>3</sub> δ): 7.76 (1H, d, j = 3.1 Hz), 7.75 (1H, d, j = 3.3 Hz), 7.60 – 7.64 (6H, m), 7.52 – 7.55 (4H, m), 7.02 (2H, d, j = 9.0 Hz), 6.67 – 6.70 (2H, m), 3.88 (3H, s), 3.67 (2H, br), 1.90 – 2.07 (8H, m), 1.08 – 1.28



(40H, m), 0.77 – 0.83 (20H, m). MS (HABA) ( $m/z$ ): 899.836.

**Compound (6).** A mixture of 3,4,9,10-perylene-tetracarboxylic acid dianhydride (**13**) (0.39 g, 0.994 mmol) 7'-(4-methoxyphenyl)-9,9,9',tetraoctyl-[2,2']-bifluorenyl-7-ylamine (**32**) (1.87 g, 2.10 mmol) zinc acetate dihydrate (0.11 g, 0.497 mmol) and imidazole (8.00 g) was heated at 160 °C overnight. The cooled reaction mixture was extracted into dichloromethane (4 x 50 cm<sup>3</sup>) and the resultant solution filtered to remove the precipitate formed. The filtrate was concentrated under reduced pressure and the crude product purified by column chromatography on silica gel, using dichloromethane as eluent and recrystallisation from a mixture of dichloromethane and dimethyl sulphoxide to yield a red crystalline solid (0.62 g, 29%). <sup>1</sup>H NMR (400 MHz, CDCl<sub>3</sub> δ): 8.80 (4H, d,  $j = 7.9$  Hz), 8.73 (4H, d,  $j = 8.4$  Hz), 7.93 (2H, d,  $j = 8.4$  Hz), 7.85 (2H, d,  $j = 7.9$  Hz), 7.79 (4H, t,  $j = 8.5$  Hz), 7.62 – 7.71 (12H, m), 7.55 – 7.57 (4H, m), 7.35 – 7.37 (4H, m), 7.03 (4H, d,  $j = 8.8$  Hz), 3.89 (6H, s), 2.05 – 2.08 (16H, m), 1.10 – 1.24 (80H, m), 0.79 – 0.90 (40H, m). MS (HABA) ( $m/z$ ): 2156.907 Anal. Calc. C: 85.75, H: 8.50, N: 1.30 Anal. Obt. C: 86.13, H: 8.09, N: 1.34. Trans. Temp. Cr - SmC = 229 °C; SmC - I = 183 °C.

### 3. Results and Discussion

#### 3.1 Mesophase Identification.

[Insert Table 1 here]

The liquid crystalline transition temperatures and melting points of the compounds **1-6**

were investigated using a combination of differential scanning calorimetry (DSC) and optical microscopy between crossed polarizers. Compounds **1**, **2**, **4** and **5** do not exhibit observable liquid crystalline phases and just melt at 274 °C, 182 °C, 261 °C and 348°C respectively, to form an isotropic liquid, see table 1. Only compounds **3** and **6** exhibit thermotropic liquid crystalline mesophases. Compound **3** forms a nematic phase, above the high melting point of 285 °C; bright nematic droplets were observed with the polarizing microscope on cooling compound **3** from the black isotropic liquid to form a highly birefringent Schlieren texture with two and four-point brushes characteristic of the nematic phase. Some optically extinct homeotropic areas are also present in the sample observed and as the sample was cooled further the texture often formed more of these optically extinct homeotropic areas. This behavior indicates that the observed phase is optically uniaxial. Both the birefringent and homeotropic areas flash brightly under mechanical disturbance, which along with the simultaneous presence of both the homeotropic texture and the Schlieren texture, confirms that the mesophase observed is a nematic phase. Compound **6** only exhibits a monotropic smectic C liquid crystal and forms a metastable supercooled LC phase in a thin film for room temperature processing. The smectic C phase formed on supercooling the sample from the isotropic liquid also exhibits a Schlieren texture, but only with four point brushes and no two point brushes. There are no isotropic areas due to the biaxial nature of the smectic C phase. These visual observations were confirmed by analysis of compounds **3** and **6** using DSC, which was also used to determine the glass transition temperature ( $t_g$ ). There was good agreement ( $\approx 1-2$  °C) between those values determined by optical microscopy for the liquid crystalline transitions (SmC-I and N-I) and those obtained using DSC analysis. The DSC values were determined twice on heating and cooling cycles on the same sample. The values obtained on separate samples of compounds **3**

and **6** are reproducible. No thermal degradation of the sample is observed even at relatively high temperatures. The base line of the spectra is relatively flat in each case and sharp transition peaks are observed for materials **3** and **6**. Both the nematic-isotropic liquid crystalline transition (N-I) and the smectic-isotropic transition (SmC-I) are first order as expected. A significant degree of supercooling below the melting point is observed on the cooling cycle and compounds **3** and **6** remain in the nematic glassy state at room temperature without crystallizing. This behavior may be attributed, at least in part, to the high viscosity of the nematic and smectic C phases of the compounds **3** and **6**, respectively, both of which has a very long molecular core with eight aliphatic chains in lateral positions and two methoxy chains in terminal positions in the case of compound **6**. Both compounds **3** and **6** contain the perylene moiety as well as four fluorene moieties. These very large, highly conjugated molecular cores also contribute to a very high viscosity of the isotropic melt. This combination of molecular components may well explain the formation of the glassy state on rapid cooling from the isotropic liquid formed above the melting point.

A spectrum of physical properties of the electron-acceptors **1-6** were investigated in order to identify the most promising candidate for fabricating bilayer photovoltaic devices with the liquid crystalline electron donor compound **7** shown in table 1. The physical properties measured include the UV-vis absorption spectra, ionization potential (IP), electron affinity (EA), energy levels, i.e., highest occupied molecular orbital (HOMO), lowest occupied molecular orbital (LUMO), band gap between them ( $E_g$ ) and the charge carrier mobility ( $\mu$ ), see below.

### 3.2. Absorption spectra.

[Insert figure 1 here]

Figure 1 shows the absorption spectrum from thin films of a selection of the perylene containing materials. The spectra show distinct transitions from the electron-donating and -accepting components of the molecules. For example, all spectra show two peaks at 495 nm and 542 nm and an accompanying shoulder at 468 nm, originating from the perylene central core, whereas the peak at 337 nm in the spectrum of compound **3** can be assigned to a transition centered on the 2,7-diphenyl-9,9-dioctylfluorenyl unit. There are no significant transitions with charge transfer character, which would be red-shifted from those localized on the individual moieties.[27] The absorption spectra show additional evidence for negligible charge transfer character; the spectra from **1** and **2** are very similar, although in the latter case the fluorene unit is decoupled from the PDI via an aliphatic spacer. The absence of a charge transfer transition suggests that the LUMO is localized on the PDI unit and the HOMO on the outer aromatic rings with no significant transition dipole moment between them. This is supported by molecular modeling of the HOMO and LUMO of **5**. As figure 2 shows, the HOMO is mainly localized on the PDI unit and the HOMO on the carbazole moiety.

[Insert figure 2 here]

### 3.3. Electrochemistry.

[Insert figure 3 and table 2 here]

The IP and EA of the compounds were found by CV. Figure 3 shows a typical CV scan showing two reversible oxidation and reduction peaks. The IP and EA of all compounds are tabulated in table 2 as well as  $E_{ox}^{onset}$ ,  $E_{red}^{onset}$  and the band-gap of the materials.  $E_g^{ec}$  is equal to IP-EA as obtained electrochemically and  $E_g^{opt}$  is the optical band-gap estimated from the absorption edge. Compound **2** has a perylene diimide core, decoupled from the fluorene units by aliphatic chains and has an EA value of 4.22 eV. In the literature there is a wide range of EA values for perylene diimide from 3.4 eV upwards.[28-31] The wide range relates to different measurement techniques and also large variations in the values of the reference potential used. Our CV experiment gives an EA value of 4.14 eV for phenyl-C61-butyric acid methyl ester (PCBM), which is within 0.15 eV of accepted value of 4.3 eV[32]. eV The EA of compounds **1 – 6** are approximately equal, suggesting that the LUMO is localized on the perylene diimide core of the molecule. The variation in values of IP supports the hypothesis that the HOMOs are centered on the outer aromatic units of the molecules. For compounds, **1-4** and **6**, which contain the fluorene unit, the IP decreases with the length of the moiety. The IP of **5** is significantly lower than that of **2** as a result of the electron-donating nature of the nitrogen atom of the carbazole unit, which replaces the fluorene moiety.[25, 33, 34] Most donor-acceptor materials have similar values of  $E_g^{ec}$  and  $E_g^{opt}$  because the charge transfer transitions originate between the HOMO and LUMO.[35, 36] Here  $E_g^{ec}$  is significantly smaller than  $E_g^{opt}$ , providing confirmation that optical transitions do not couple energy states localized on the donor and acceptor regions of the molecules. A similar result was found for a perylene-carbazole polymer.[37] The CV measurements confirm that there is no charge –transfer between the perylene core

and the electron donating moieties of compounds **1** to **6**. This is a different result to that obtained for new copolymer materials where the electron deficient perylene diimide is combined with electron donating units such as fluorene, and carbazole and some charge transfer is observed.[38, 39] Interestingly the performance of photovoltaic devices where the copolymers were used as the acceptor unit did not systematically vary with their internal charge transfer properties. The IP of the electron donor material **7** is 5.52 eV.

### **3.4. Charge transport.**

[Insert figure 4 here]

Figure 4 shows typical time-of-flight traces for hole and electron photocurrents for samples **1** and **6**. The photocurrent is measured as a function of reduced time ( $\text{time}/d$ ) and the same electric field was used for each measurement. Therefore the different reduced time-of-flight for the different samples shown in the figure reflects differences in mobility rather than in sample thickness. The transients for sample **1** have been offset  $\times 50$  for clarity. Both materials show dispersive transport so a log-log scale is needed to show well defined reduced times-of-flight, the hole transit time for both materials being indicated by arrows. The reduced transit times for both electrons and holes are over an order of magnitude smaller for sample **6** than for sample **1**. As figure 4 shows, all transients show a gradual reduction in photocurrent before the reduced transit times, with a change of slope occurring at early reduced times ( $< 10^{-6} \text{ s } \mu\text{m}^{-1}$ ). Positive and negative carriers are generated by absorption over a short distance near the incident electrode, and they travel in different directions according to the direction of the applied field. Hence the change of slope may occur when all carriers have reached the near

electrode and the continued reduction in photocurrent later results from carrier trapping.

[Insert figure 5 here]

Figure 5 shows the mobility as a function of electric field for both electrons and holes for compounds **1-3**, **5** and **6**. We were unable to make a sufficiently thick sample of compound **4** for measurement. We consider hole and electron mobility separately. The hole mobility for all the perylene compounds is low  $\leq 10^{-4} \text{ cm}^2 \text{ V}^{-1} \text{ s}^{-1}$ . However there are variations over nearly three orders of magnitude between the various materials with increases in the order  $\mathbf{5} < \mathbf{1} < \mathbf{2} \ll \mathbf{3} \approx \mathbf{6}$ . Compounds **1**, **2** and **5** have donor components with two conjugated rings only and so have the smallest mobility; transport via the fluorene unit is enhanced when it is decoupled from the perylene moiety in compound **2** while hole mobility is lowest in compound **5** despite the relatively high HOMO energy of the carbazole units. Compounds **3** and **6** have much higher hole mobilities probably because of their liquid crystalline organization; their extended hole transporting components of the molecules gives an increased probability of overlap and hopping between neighbors.

The wide variation in electron mobility, over two orders of magnitude, is more surprising, given the similar LUMO energy of all compounds and the same perylene electron transporting unit. Given that the donor-acceptor intra-molecular coupling is small as discussed above, we attribute the variations in mobility to different intermolecular coupling between neighbors. The electron mobility of **2** is over ten times greater than that of **1** suggesting that intermolecular coupling is increased when the electron and hole transporting units are separated by aliphatic chains. Interestingly the

electron mobility of **3** is over twenty times lower than that of **6** despite their similar hole mobilities. The higher mobility of **6** may relate to its smectic liquid crystalline organization. Although bulk films have monotropic smectic phase (seen only on cooling) thin films show LC phases when formed by solution processing. This may improve intermolecular coupling between neighboring perylene units. The electron mobility of **6** compares well to that of the compound (3,4,5Pr)<sub>12</sub>G1-3-perylenetetracarboxyldiimide which has a columnar phase at room temperatures with a mobility of  $\approx 3 \times 10^{-5} \text{ cm}^2 \text{ V}^{-1} \text{ s}^{-1}$ . [40] Elsewhere it was found that the mobility of discotic perylene materials varied enormously with processing conditions. [41]

### 3.5. Bilayer Photovoltaic devices.

[Insert figure 6 and table 3 here]

Figure 6 shows the photocurrent- voltage characteristics of bilayer photovoltaic devices having the same donor **7** and different acceptors, **1**, **3**, **4** and **5**, on irradiation with  $\sim 24 \text{ mW/cm}^2$  of light of wavelength 465 nm. The donor and acceptor were deposited from 1.5 wt% and 1.0 wt % solutions in chlorobenzene respectively. Table 3 summarizes the performance of the devices. The short-circuit current density is  $J_{SC}$ , the open-circuit voltage is  $V_{OC}$  and the power conversion efficiency  $\eta_P$  is defined as

$$\eta_P = \frac{V_{\max} J_{\max}}{I_{inc}} = \frac{FF \times V_{OC} J_{SC}}{I_{inc}} \quad (1)$$

where  $I_{inc}$  is the optical irradiance incident to the photovoltaic cell. The fill factor,  $FF$ , is the ratio of the maximum power rectangle  $V_{\max} \times J_{\max}$  to the rectangle  $V_{OC} \times J_{SC}$ . The series resistance ( $R_S$ ) results from the finite conductivity of the semiconducting material,



the contact resistance between the semiconductors and the electrodes, as well as the resistance associated with electrodes and interconnections. The shunt resistance ( $R_P$ ) results from the loss of carriers via possible leakage paths. These paths include collection at the wrong electrode giving continuous pathways for both electrons and holes between the anode and cathode, structural defects such as pinholes in the film or recombination centres. The parameter “ $n$ ”, is the index in the formula  $J_{SC} = a \cdot I_{inc}^n$  where  $a$  is a constant. In all cases  $V_{oc}$  approaches the difference, to within 0.2 V, between the HOMO of the donor and the LUMO of the acceptor. The differences in performance of the devices relate mostly to  $J_{SC}$  and the  $FF$ . Acceptor **1** has a higher electron mobility than that of **3** and **5**, which may account for the better performance of the **7:1** device. However, device **7:5** is significantly better than **7:3** despite the similar values of electron mobility for both acceptors. A rule of thumb is that the value of  $R_S$  must be small compared to the characteristic resistance defined as  $R_{CH} = V_{OC}/I_{SC}$  while  $R_P$  must be large compared to  $R_{CH}$ .<sup>[42]</sup> All devices, particularly **7:4**, have high values of  $R_S$  and low values of  $R_P$ . In all devices  $n > 0.9$  showing the recombination is mostly monomolecular (geminate).

Table 4 compares the performance of bilayer devices, all based on the **7:1** combination with different layer thickness. The layer thickness depends on the concentration (given in % weight of solution) of the solution used for spin-casting. It suggests that the high  $R_S$ , low  $R_P$  and low  $FF$  are related to the poor electron mobility,  $< 10^{-5} \text{ cm}^2 \text{ V}^{-1} \text{ s}^{-1}$ , of the acceptor **1**: These parameters change substantially when the acceptor is deposited from a solution concentration of 2.0wt % compared to 1.0 wt %. Note also that the former device has substantially more bimolecular recombination. Changing the concentration of the donor solution between 1.5 and 2.5 weight % has a much smaller effect on device

performance, possibly because of the relatively high hole mobility of **7**.

The performance deteriorates as the thickness of the blend increases. There are some striking albeit expected differences between the blend and bilayer devices. The  $FF$  and  $R_p$  are worse for the blend devices suggesting the need of barrier layers to ensure that carriers cannot reach the wrong contact. The blend photovoltaics show significantly more bimolecular recombination than the bilayer devices as indicated by the consistently low value of  $n$  for the former. This results from non-geminate recombination, possibly at the heterojunctions of domains which are disconnected from electrodes. The generation of space-charge caused by a large difference between electron and hole mobility would also increase the rate of non-geminate recombination.

Of necessity, the donor layer of all of the bilayer devices is crosslinked by irradiation with ultraviolet light to obtain an insoluble layer before depositing the acceptor layer.

We now show that crosslinking does not degrade device performance. Two bulk heterojunction devices containing a single layer of a 1:1 (by weight) blend of **7** and **1** were prepared using identical conditions except that one was irradiated with ultraviolet light of fluence  $300 \text{ J cm}^{-2}$  before deposition of the top electrode. This resulted in crosslinking of the donor material only which has photopolymerizable end-groups.

Analysis using atomic force microscopy suggests that the domain size of the bulk heterojunction was unchanged by photopolymerisation.[22, 43] This is not surprising since the thin film is in a glassy solid state at room temperature so that there is minimal material movement during polymerization.[43] Within experimental error, the performance of both devices was identical showing that crosslinking does not degrade performance. Interestingly the “ $n$ ” parameter of the blended devices was significantly lower, equal to 0.67, than that of the bilayer devices showing more bimolecular

recombination

#### **4. Conclusion**

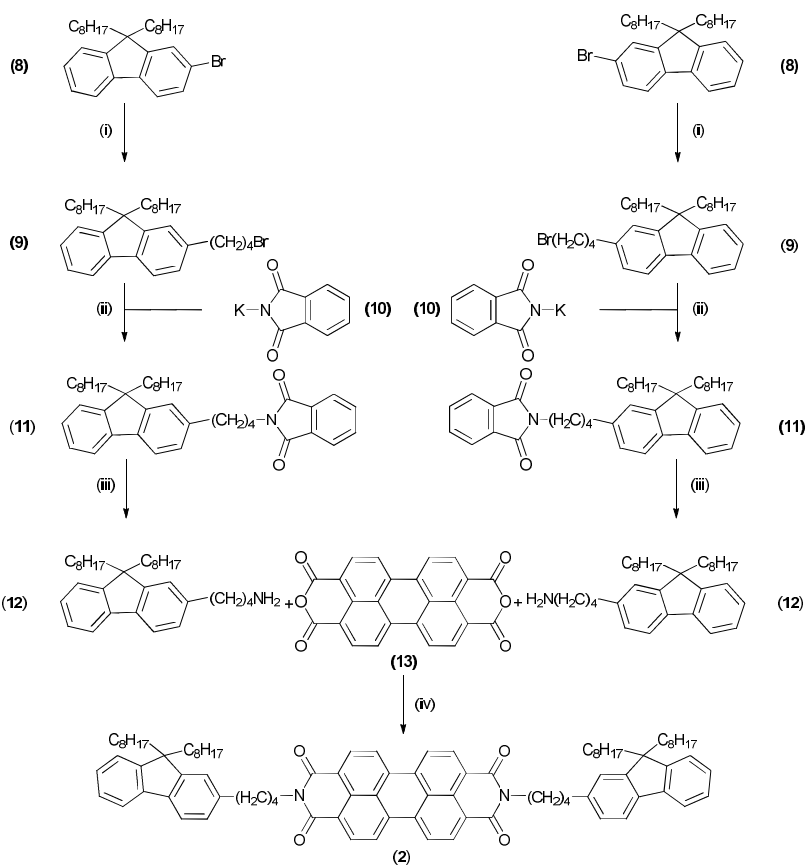
We demonstrate solution processed bilayer organic photovoltaics, where the lower electron donating layer is crosslinked by photopolymerisation prior to depositing a perylene based acceptor layer on top. These results demonstrate the potential of crosslinking of reactive mesogens as a promising solution-processable route to multilayer photovoltaics. It is particularly noteworthy that the performance of the crosslinked and non-crosslinked blended devices are similar, allaying fears that crosslinking would cause photodegradation. Further work is required to significantly improve the series and parallel resistances of the devices by the development of electron accepting materials with higher mobility and by the improvement of contact interfaces.

Acknowledgements: G. Sowersby is thanked for technical support. We acknowledge the EPSRC for financial support.

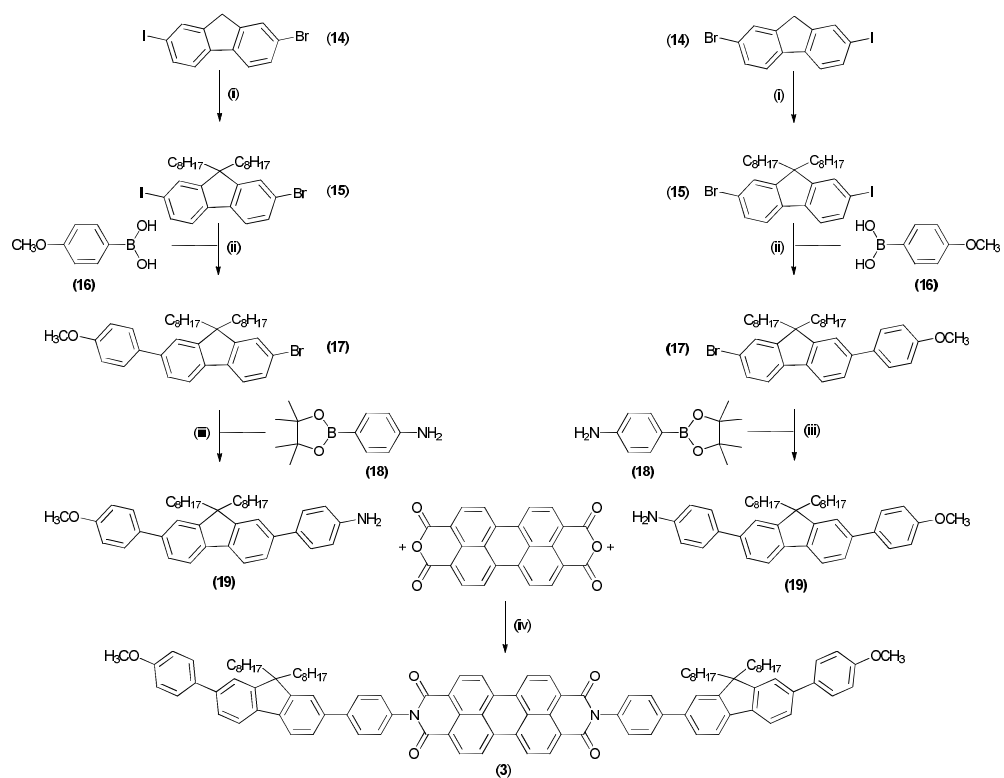
1. Halls JJM, Walsh CA, Greenham NC, Marseglla EA, Friend RH, Moratti SC, et al. Efficient photodiodes from interpenetrating polymer networks. *Nature*. 1995;376(6540):498-500.
2. Yu G, Gao J, Hummelen JC, Wudl F, Heeger AJ. Polymer photovoltaic cells: Enhanced efficiencies via a network of internal donor-acceptor heterojunctions. *Science*. 1995;270(5243):1789-91.
3. Tang CW. Two-layer organic photovoltaic cell. *ApplPhys Lett*. 1986;48:183.
4. Park SH, Roy A, Beaupré S, Cho S, Coates N, Moon JS, et al. Bulk heterojunction solar cells with internal quantum efficiency approaching 100%. *Nature Photonics*. 2009;3(5):297-303.
5. Chen HY, Hou J, Zhang S, Liang Y, Yang G, Yang Y, et al. Polymer solar cells with enhanced open-circuit voltage and efficiency. *Nature Photonics*. 2009;3(11):649-53.
6. Liang Y, Xu Z, Xia J, Tsai ST, Wu Y, Li G, et al. For the bright future-bulk heterojunction polymer solar cells with power conversion efficiency of 7.4%. *Advanced Materials*. 2010;22(20):E135-E8.
7. Brabec CJ, Gowrisanker S, Halls JJM, Laird D, Jia S, Williams SP. Polymer-fullerene bulk-heterojunction solar cells. *Advanced Materials*. 2010;22(34):3839-56.
8. Liang Y, Yu L. A new class of semiconducting polymers for bulk heterojunction solar cells with exceptionally high performance. *Accounts of Chemical Research*. 2010;43(9):1227-36.
9. Peumans P, BuloviÄ V, Forrest SR. Efficient photon harvesting at high optical intensities in ultrathin organic double-heterostructure photovoltaic diodes. *Applied Physics Letters*. 2000;76(19):2650-2.
10. Peumans P, Yakimov A, Forrest SR. Small molecular weight organic thin-film photodetectors and solar cells. *Journal of Applied Physics*. 2003;93(7):3693-723.
11. Xue J, Uchida S, Rand BP, Forrest SR. Asymmetric tandem organic photovoltaic cells with hybrid planar-mixed molecular heterojunctions. *Applied Physics Letters*. 2004;85(23):5757-9.
12. Droege S, Khalifah MSA, O'Neill M, Thomas HE, Simmonds HS, Macdonald JE, et al. Grazing incidence X-ray diffraction of a photoaligned nematic semiconductor. *Journal of Physical Chemistry B*. 2009;113(1):49-53.
13. Aldred MP, Vlachos P, Contoret AEA, Farrar SR, Chung-Tsoi W, Mansoor B, et al. Linearly polarised organic light-emitting diodes (OLEDs): synthesis and characterisation of a novel hole-transporting photoalignment copolymer. *J Mater Chem*. 2005;15(31):3208-13. doi: 10.1039/b50603j. PubMed PMID: ISI:000231247000006.
14. Contoret AEA, Farrar SR, Jackson PO, Khan SM, May L, O'Neill M, et al. Polarized electroluminescence from an anisotropic nematic network on a non-contact photoalignment layer. *Adv Mater*. 2000;12(13):971-+. PubMed PMID: ISI:000088290700009.
15. Woon KL, Contoret AEA, Farrar SR, Liedtke A, O'Neill M, Vlachos P, et al. Material and device properties of highly birefringent nematic glasses and polymer networks for organic electroluminescence. *J Soc Inf Disp*. 2006;14(6):557-63. PubMed PMID: ISI:000244853100008.
16. Aldred MP, Eastwood AJ, Kelly SM, Vlachos P, Contoret AEA, Farrar SR, et al. Light-emitting fluorene photoreactive liquid crystals for organic electroluminescence. *Chem Mat*. 2004;16(24):4928-36. doi: 10.1021/cm0351893. PubMed PMID: ISI:000225365800014.

17. Contoret AEA, Farrar SR, O'Neill M, Nicholls JE. The photopolymerization and cross-linking of electroluminescent liquid crystals containing methacrylate and diene photopolymerizable end groups for multilayer organic light-emitting diodes. *Chem Mat.* 2002;14(4):1477-87. doi: 10.1021/cm011111f. PubMed PMID: ISI:000175028700007.
18. McCulloch I, Zhang W, Heeney M, Bailey C, Giles M, Graham D, et al. Polymerisable liquid crystalline organic semiconductors and their fabrication in organic field effect transistors. *Journal of Materials Chemistry.* 2003;13(10):2436-44.
19. Liedtke A, O'Neill M, Kelly SM, Kitney SP, Van Averbeke B, Boudard P, et al. Optical properties of Light-Emitting Nematic Liquid Crystals: A Joint Experimental and Theoretical Study. *J Phys Chem B.* 2010;114:11975-82.
20. Woon KL, Aldred MP, Vlachos P, Mehl GH, Stirner T, Kelly SM, et al. Electronic charge transport in extended nematic liquid crystals. *Chem Mat.* 2006;18(9):2311-7. doi: 10.1021/cm0601335. PubMed PMID: ISI:000237389700017.
21. Carrasco-Orozco M, Tsoi WC, O'Neill M, Aldred MP, Vlachos P, Kelly SM. New photovoltaic concept: Liquid-crystal solar cells using a nematic gel template. *Adv Mater.* 2006;18(13):1754-+. doi: 10.1002/adma.200502008. PubMed PMID: ISI:000239181300024.
22. Tsoi WC, O'Neill M, Aldred MP, Kitney SP, Vlachos P, Kelly SM. Distributed bilayer photovoltaics based on nematic liquid crystal polymer networks. *Chem Mat.* 2007;19(23):5475-84. doi: 10.1021/cm071727q. PubMed PMID: ISI:000250803900004.
23. Tsoi WC, O'Neill M, Aldred MP, Vlachos P, Kelly SM. Triplets in extended nematic liquid crystals and polarons in their blends. *J Chem Phys.* 2007;127(11). doi: 114901  
10.1063/1.2768346. PubMed PMID: ISI:000249667400059.
24. Bard AJ, Faulkner LR. *Electrochemical methods : fundamentals and applications.* Second ed. New York: John Wiley; 2001.
25. Van Dijken A, Bastiaansen JJAM, Kigger NMM, Langeveld BMW, Rothe C, Monkman A, et al. Carbazole compounds as host materials for triplet emitters in organic light-emitting diodes: Polymer hosts for high-efficiency light-emitting diodes. *Journal of the American Chemical Society.* 2004;126(24):7718-27.
26. AlKhalifah MS. *Nematic Liquid Crystals for Nano-Structured Organic Photovoltaics* University of Hull; 2009.
27. Zhan X, Tan Z, Zhou E, Li Y, Misra R, Grant A, et al. Copolymers of perylene diimide with dithienothiophene and dithienopyrrole as electron-transport materials for all-polymer solar cells and field-effect transistors. *Journal of Materials Chemistry.* 2009;19(32):5794-803.
28. Schmidt-Mende L, Fechtenkötter A, Müllen K, Moons E, Friend RH, MacKenzie JD. Self-organized discotic liquid crystals for high-efficiency organic photovoltaics. *Science.* 2001;293(5532):1119-22.
29. Pommerehne J, Vestweber H, Guss W, Mahrt RF, Bäßler H, Porsch M, et al. Efficient two layer LEDs on a polymer blend basis. *Advanced Materials.* 1995;7(6):551-4.
30. Erten S, Meghdadi F, Gunes S, Koeppe R, Sariciftci NS, Icli S. Donor-acceptor heterojunction solar cells based on perylene diimide and perylene bisbenzimidazole. *EPJ Applied Physics.* 2006;36(3):225-9.
31. Jones BA, Ahrens MJ, Yoon MH, Facchetti A, Marks TJ, Wasielewski MR. High-mobility air-stable n-type semiconductors with processing versatility: Dicyanoperylene-3,4:9,10-bis(dicarboximides). *Angewandte Chemie - International Edition.* 2004;43(46):6363-6.

32. Dennler G, Scharber MC, Brabec CJ. Polymer-fullerene bulk-heterojunction solar cells. *Advanced Materials*. 2009;21(13):1323-38.
33. Brunner K, Van Dijken A, Bäumer H, Bastiaansen JJAM, Kigger NMM, Langeveld BMW. Carbazole Compounds as Host Materials for Triplet Emitters in Organic Light-Emitting Diodes: Tuning the HOMO Level without Influencing the Triplet Energy in Small Molecules. *Journal of the American Chemical Society*. 2004;126(19):6035-42.
34. Stephan O, Vial JC. Blue light electroluminescent devices based on a copolymer derived from fluorene and carbazole. *Synthetic Metals*. 1999;106(2):115-9.
35. Karsten BP, Viani L, Gierschner J, Cornil J, Janssen RAJ. On the origin of small band gaps in alternating thiophene - thienopyrazine oligomers. *Journal of Physical Chemistry A*. 2009;113(38):10343-50.
36. Li Y, Xue L, Li H, Li Z, Xu B, Wen S, et al. Energy level and molecular structure engineering of conjugated donor-acceptor copolymers for photovoltaic applications. *Macromolecules*. 2009;42(13):4491-9.
37. Koyuncu S, Zafer C, Koyuncu FB, Aydin B, Can M, Sefer E, et al. A New donor-acceptor double-cable carbazole polymer with perylene bisimide pendant group: Synthesis, electrochemical, and photovoltaic properties. *Journal of Polymer Science, Part A: Polymer Chemistry*. 2009;47(22):6280-91.
38. Zhou E, Cong J, Wei Q, Tajima K, Yang C, Hashimoto K. All-polymer solar cells from perylene diimide based copolymers: Material design and phase separation control. *Angewandte Chemie - International Edition*. 2011;50(12):2799-803.
39. Zhou E, Tajima K, Yang C, Hashimoto K. Band gap and molecular energy level control of perylene diimide-based donor-acceptor copolymers for all-polymer solar cells. *Journal of Materials Chemistry*. 2010;20(12):2362-8.
40. Duzhko V, Aqad E, Imam MR, Peterca M, Percec V, Singer KD. Long-range electron transport in a self-organizing n-type organic material. *Applied Physics Letters*. 2008;92(11).
41. An Z, Yu J, Jones SC, Barlow S, Yoo S, Domercq B, et al. High electron mobility in room-temperature discotic liquid-crystalline perylene diimides. *Advanced Materials*. 2005;17(21):2580-3.
42. Kippelen B, Bradley JJ. Organic photovoltaics. *Energy and Environmental Science*. 2009;2(3):251-61.
43. Liedtke A, Chunhong L, O'Neill M, Dyer PE, Kitney SP, Kelly SM. One-Step Photoembossing for Submicrometer Surface Relief Structures in Liquid Crystal Semiconductors. *ACS Nano*. 2010;4(6):3248-53. Epub May 2010. doi: 10.1021/nn100012g.

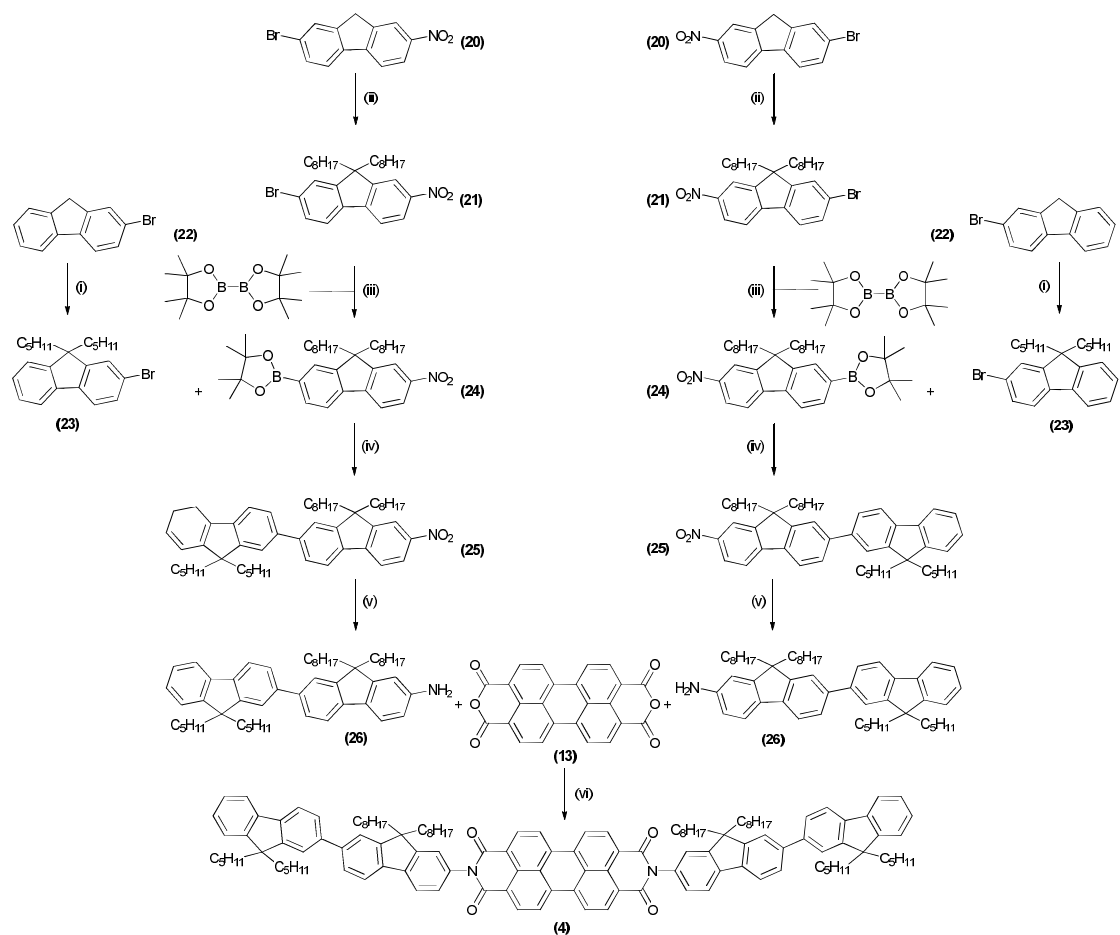


**Scheme 1.** Reagents and conditions (i) a) *n*-BuLi, EtOEt, -78 °C, b) BrC<sub>4</sub>H<sub>8</sub>Br, (ii) Toluene, 120 °C, (iii) H<sub>2</sub>NNH<sub>2</sub>.H<sub>2</sub>O, EtOH, 65 °C, (iv) Imadazole, Zn(OAc)<sub>2</sub>.2H<sub>2</sub>O, (CH<sub>3</sub>)<sub>2</sub>NCOCH<sub>3</sub>, 180 °C.

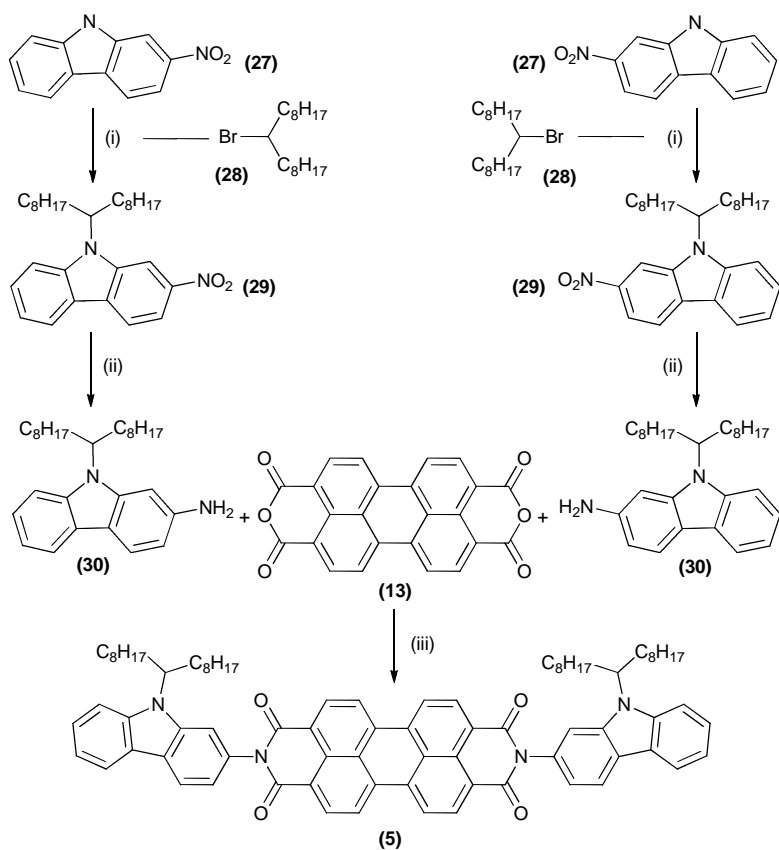


**Scheme 2.** Reagents and conditions (i) KOH, KI, DMSO,  $C_8H_{17}Br$  (ii)  $K_2CO_3$ ,  $Pd(PPh_3)_4$ , THF, 75 °C, (iii) DMF,  $K_3PO_4$ ,  $Pd(PPh_3)_4$ , DMF, 100 °C, (iv) Imadazole,  $Zn(OAc)_2 \cdot 2H_2O$ ,  $(CH_3)_2NCOCH_3$ , 180 °C.

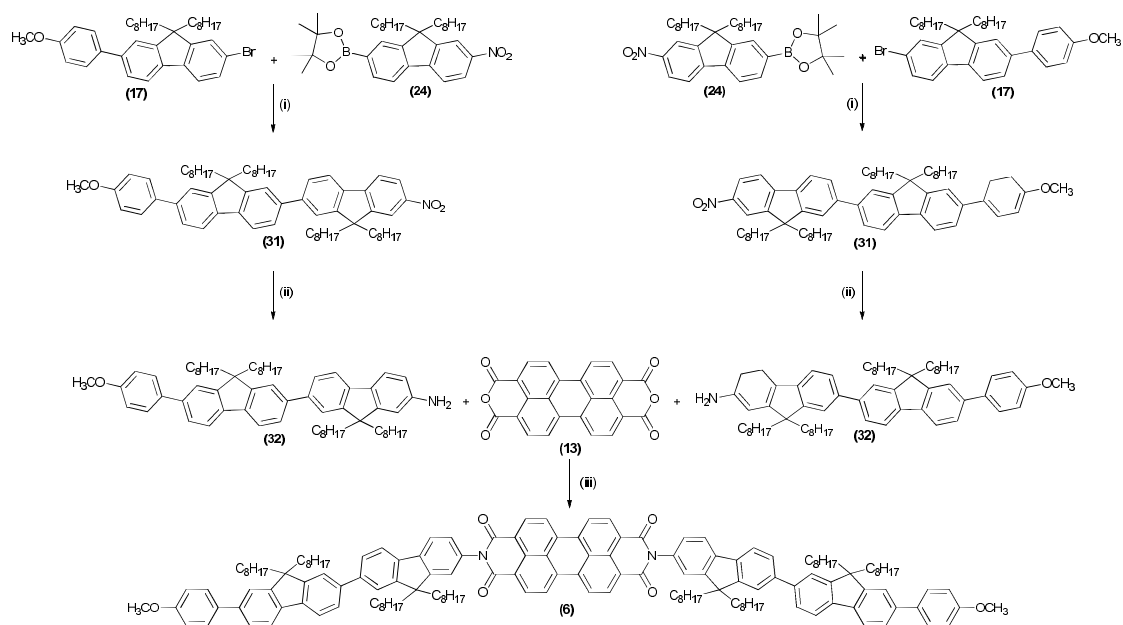




**Scheme 3.** Reagents and conditions (i) KOH, KI, DMSO, C<sub>5</sub>H<sub>11</sub>Br (ii) KOH, KI, DMSO, C<sub>8</sub>H<sub>17</sub>Br (iii) CH<sub>3</sub>CO<sub>2</sub>K, DMSO, 80 °C (iv) K<sub>2</sub>PO<sub>3</sub>, Pd(PPh<sub>3</sub>)<sub>4</sub>, DMSO, 80 °C, (v) SnCl<sub>2</sub>·2H<sub>2</sub>O, EtOH, 65 °C, (vi) Imadazole, Zn(OAc)<sub>2</sub>·2H<sub>2</sub>O, (CH<sub>3</sub>)<sub>2</sub>NCOCH<sub>3</sub>, 180 °C.



**Scheme 4.** Reagents and conditions (i) KOH, DMSO (ii) SnCl<sub>2</sub>.2H<sub>2</sub>O, EtOH, 65 °C, (iii) Imadazole, Zn(OAc)<sub>2</sub>.2H<sub>2</sub>O, (CH<sub>3</sub>)<sub>2</sub>NCOCH<sub>3</sub>, 180 °C.



**Scheme 5.** Reagents and conditions (i)  $K_2PO_3$ ,  $Pd(PPh_3)_4$ , DMF, 80 °C, (ii)

$SnCl_2 \cdot 2H_2O$ , EtOH, 65 °C, (iii) Imadazole,  $Zn(OAc)_2 \cdot 2H_2O$ ,  $(CH_3)_2NCOCH_3$ , 180 °C.

Table 1. The chemical structure of the compounds used in this investigation and their liquid crystalline transition temperatures.

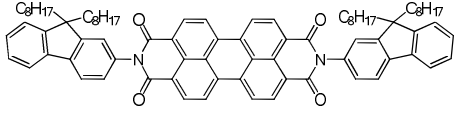
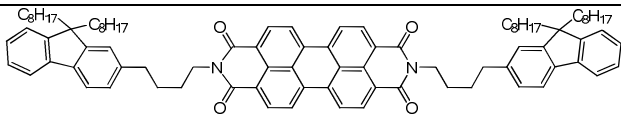
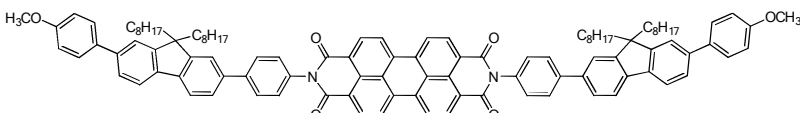
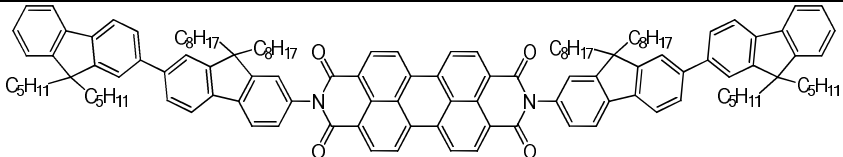
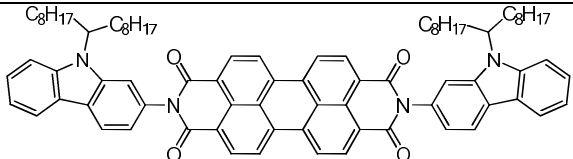
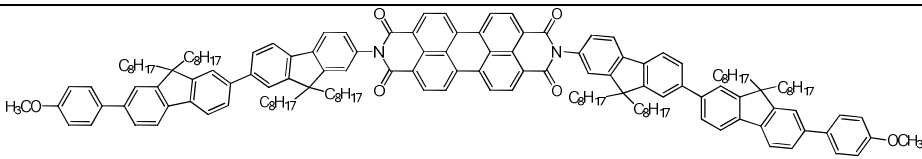
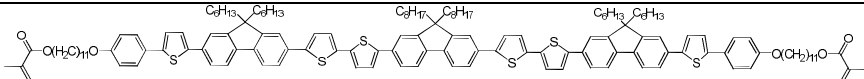
1	 <p style="text-align: right;">Cr-I = 274 °C</p>
2	 <p style="text-align: right;">Cr-I = 182 °C</p>
3	 <p style="text-align: right;">Cr-N = 285 °C N-I = &gt;350 °C</p>
4	 <p style="text-align: right;">Cr-I = 261 °C</p>
5	 <p style="text-align: right;">Cr-I = 348 °C</p>
6	 <p style="text-align: right;">Cr-I = 229 °C; SmC-I = 183 °C</p>
7	 <p style="text-align: right;">Tg = 23 °C; Cr-N = 151 °C</p>

Table 2. The onset oxidation and reduction potentials,  $E_{ox}^{onset}$  and  $E_{red}^{onset}$ , measured with reference to the Ag/AgCl electrode, ionization potential (IP), electron affinity (EA) for compounds **1-7**. The electrochemical band-gap is  $E_g^{ec} = IP - EA$ . The optical band-gap,  $E_g^{opt}$ , is found from the absorption edge.

	$E_{ox}^{onset}$ (V)	$E_{red}^{onset}$ (V)	IP	EA	$E_g^{ec}$ (eV)	$E_g^{opt}$ (eV)
<b>1</b>	-	-0.51	-	4.19	-	2.12
<b>2</b>	1.49	-0.48	6.19	4.22	1.97	2.10
<b>3</b>	1.19	-0.45	5.89	4.25	1.64	2.12
<b>4</b>	1.28	-0.49	5.98	4.21	1.77	2.12
<b>5</b>	0.85	-0.47	5.55	4.23	1.32	2.06
<b>6</b>	1.15	-0.48	5.85	4.20	1.65	2.12
<b>7</b>	0.82	-	5.52	-	-	2.33

Table 3. Performance parameters of bilayer photovoltaic devices with the same donor **7** and different acceptors. The devices were illuminated with light of irradiance  $\sim 24$  mW/cm<sup>2</sup> and wavelength 465 nm.

<b>D:A</b>	$\eta_P$ (%)	FF (%)	$I_{SC}$ (mA cm <sup>-2</sup> )	$V_{OC}$ (V)	$R_S$ (k $\Omega$ cm <sup>2</sup> )	$R_P$ (k $\Omega$ cm <sup>2</sup> )	$n$
<b>7:1</b>	0.93	36	0.50	1.2	1.1	6.0	0.96
<b>7:3</b>	0.53	32	0.36	1.1	1.8	4.8	0.94
<b>7:4</b>	0.42	28	0.31	1.15	3.7	4.7	0.91
<b>7:5</b>	0.63	33	0.40	1.15	1.9	5.0	0.94

Table 4. Performance parameters of bilayer photovoltaic devices with the same donor **7** and acceptor **1** but prepared with different concentration of the donor:acceptor spin-cast solutions given in column 1 as the weight % in solvent. The devices were illuminated with light of irradiance  $\sim 24\text{mW/cm}^2$  and wavelength 465 nm.

<b>7:1</b> <b>Wt %</b>	$\eta_p$ (%)	FF (%)	$I_{SC}$ (mA $\text{cm}^{-2}$ )	$V_{OC}$ (V)	$R_S$ ( $\text{k}\Omega\text{cm}^2$ )	$R_P$ ( $\text{k}\Omega\text{cm}^2$ )	$n$
1.5:1.0	0.93	36	0.50	1.2	1.1	6.0	0.96
2.0:1.0	0.88	35	0.49	1.2	1.5	5.7	0.96
2.5:1.0	0.70	34	0.42	1.2	1.6	6.3	0.95
2.0:2.0	0.60	25	0.48	1.2	3.7	2.9	0.88

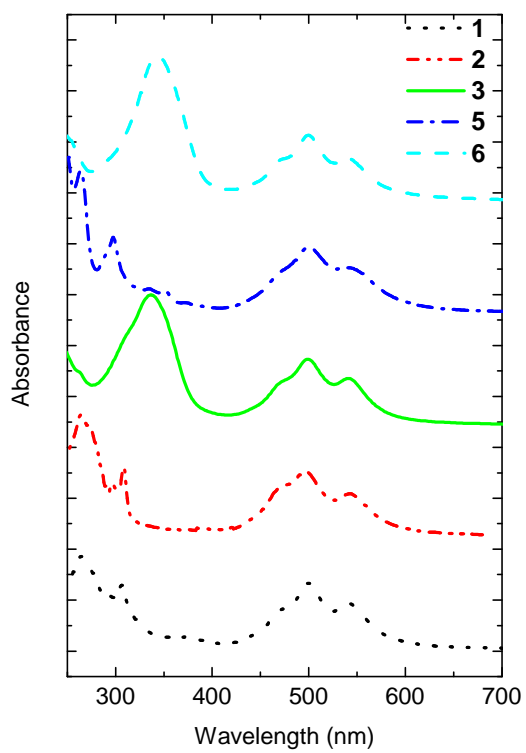
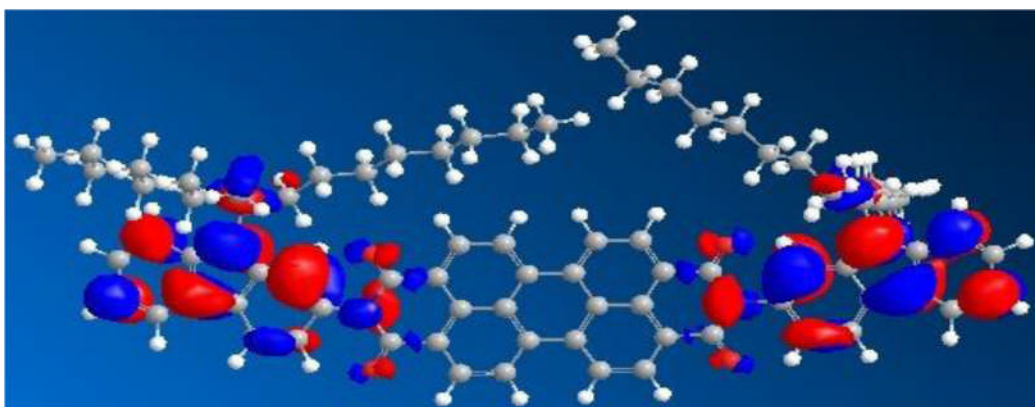


Figure 1. Absorption spectra of thin films of compounds **1-3, 5** and **6**.



a)



b)

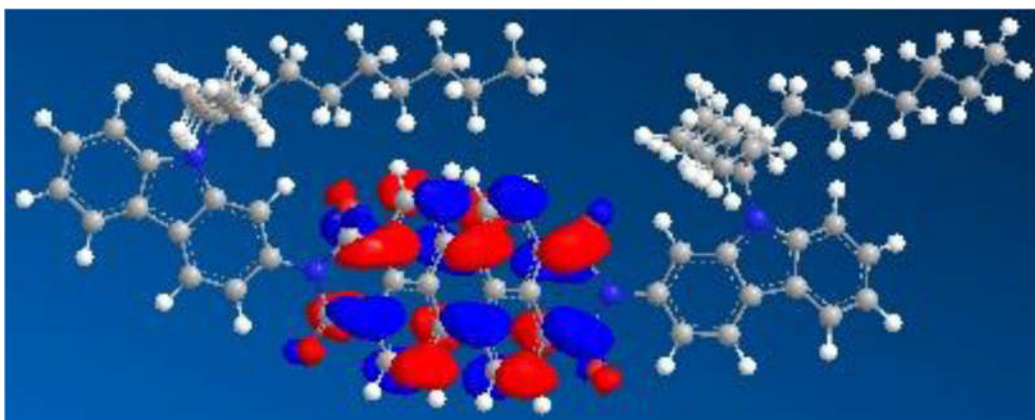


Figure 2. Molecular orbital contour plot of a) HOMO and b) LUMO levels of compound **5**.

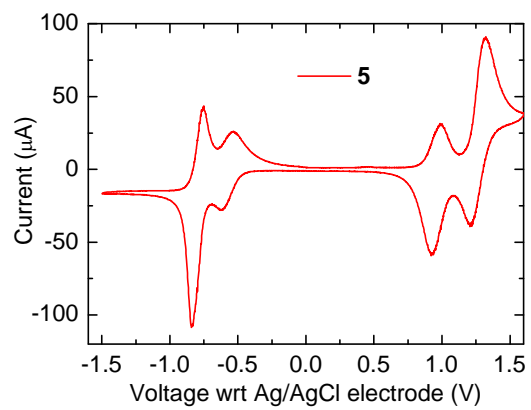


Figure 3 Cyclic voltammogram of **5** showing two reversible oxidation and reduction transitions.

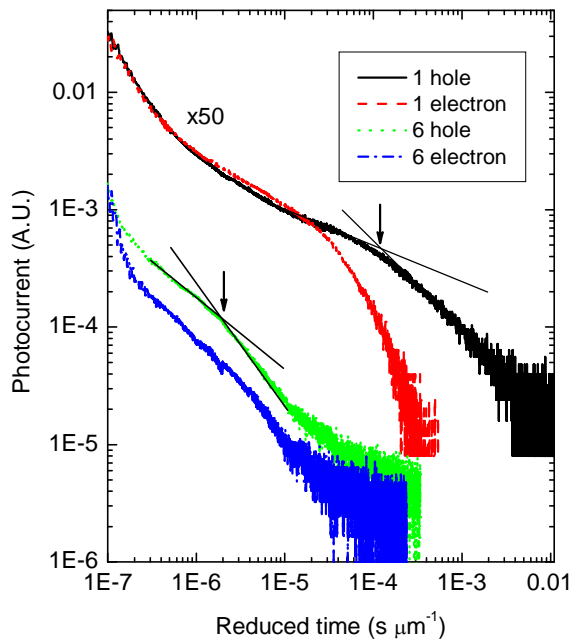


Figure 4. Electron and hole photocurrent as a function of reduced time ( $\text{time}/l$ ) for samples **1** and **6** at an electric field of  $7 \times 10^5 \text{ V cm}^{-1}$ . The photocurrents from sample **1** are multiplied  $\times 50$  for improved clarity. The reduced transit times for holes for both samples are indicated by arrows.

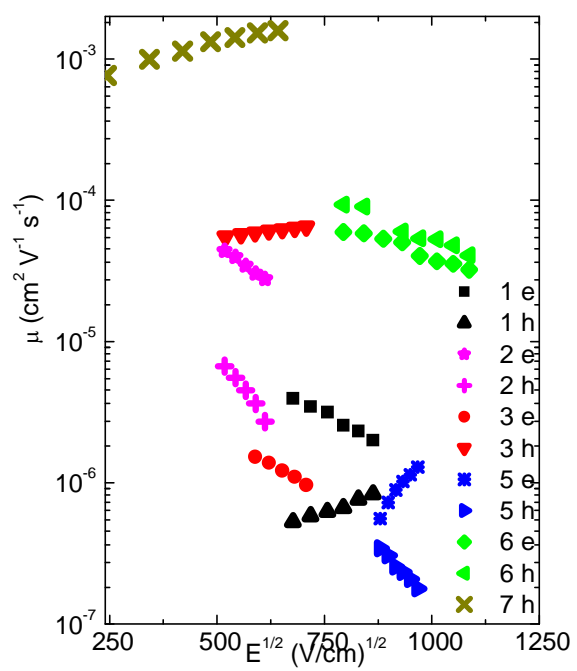


Figure 5. Room temperature mobility for holes (h) and electrons (e) of compounds **1-3**, **5**, **6** and **7** as a function of the (applied field  $E$ ) $^{1/2}$ .

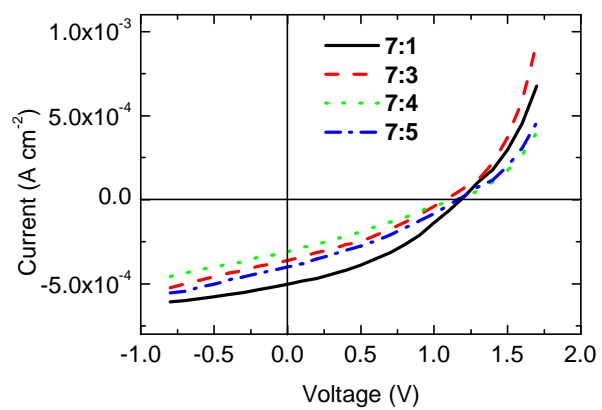


Figure 6. Photocurrent voltage characteristics of bilayer photovoltaic devices on excitation with light of irradiance  $24 \text{ mW cm}^{-2}$  and a wavelength of  $465 \pm 5 \text{ nm}$ .